

Correlations of Properties and Structures at Different Length Scales of Hydro- and Organo-gels Based on *N*-Alkyl-(*R*)-12-Hydroxyoctadecylammonium Chlorides

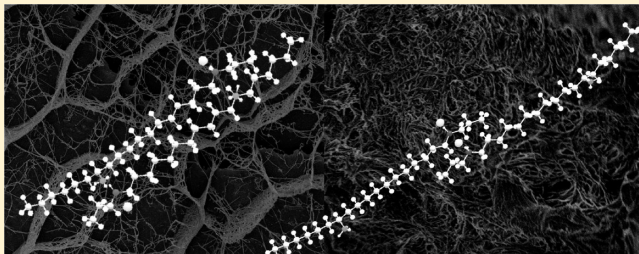
V. Ajay Mallia,[†] Pierre Terech,[‡] and Richard G. Weiss^{*†}

[†]Department of Chemistry, Georgetown University, Washington, D.C. 20057-1227, United States

[‡]SPrAM, UMR CEA/UJF-Grenoble 1, INAC, Grenoble, F-38054, France

 Supporting Information

ABSTRACT: The self-assembly and gelating ability of a set of *N*-alkyl-(*R*)-12-hydroxyoctadecylammonium chlorides ($\text{NCl}-n$, where $n = 0\text{--}6, 18$ is the length of the alkyl chain on nitrogen) are described. Several are found to be ambidextrous (gelating both water and a variety of organic liquids) and very efficient (needing less than ca. 0.5 wt % at room temperature). Structure–property correlations at different distance scales of the $\text{NCl}-n$ in their hydro- and organo-gels and neat, solid states have been made using X-ray diffraction, neutron scattering, thermal, optical, cryo-SEM and rheological techniques. The self-assembled fibrillar networks consist of spherulitic objects with fibers whose diameters and degrees of twisting differ in the hydro- and organo-gels. Increasing n (and, thus, the molecular length) increases the width of the fibers in their hydrogels; an irregular, less pronounced trend between n and fiber width is observed in the corresponding toluene gels. Time-dependent, small angle neutron scattering data for the isothermal sol-to-gel transformation of sols of $\text{NCl}-18$ /toluene to their gels, treated according to Avrami theory, indicate heterogeneous nucleation involving rodlike growth. Rheological studies of gels of $\text{NCl}-3$ in water and toluene confirm their viscoelastic nature and show that the hydrogel is mechanically stronger than the toluene gel. Models for the different molecular packing arrangements within the fibrillar gel networks of the hydro- and organogels have been inferred from X-ray diffraction. The variations in the fibrillar networks provide a comprehensive picture and detailed insights into why seemingly very similar $\text{NCl}-n$ behave very differently during their self-assembly processes in water and organic liquids. It is shown that the $\text{NCl}-n$ provide a versatile platform for interrogating fundamental questions regarding the links between molecular structure and one-dimensional self-aggregation, leading to gelation.



INTRODUCTION

Molecular gels are solidlike materials composed of a liquid and a low concentration of a low molecular-mass molecule, a gelator, which is topologically a 0-dimensional object at micrometer distance scales.¹ The gelator molecules self-assemble by one-dimensional growth modes² to form fibers, strands, tapes, or tubules that are held together via weak physical intermolecular forces (such as H-bonding, electrostatic forces, π – π stacking, and London dispersion forces) and interact physically to form 3-dimensional networks. The networks immobilize the liquid component on a macroscopic scale via surface tension and capillary forces.^{1e,3} During the past two decades, molecular gels have garnered an enormous amount of attention because of their potential and realized applications⁴ and their fundamental importance to gaining an understanding of how and why molecules aggregate in specific orientations at different distance scales.^{1,5} To exploit to the fullest extent these applications and fundamental insights, it will be necessary to identify the salient structural features that lead to efficient and versatile gelators, especially those capable of gelating both low- and high-polarity liquids.

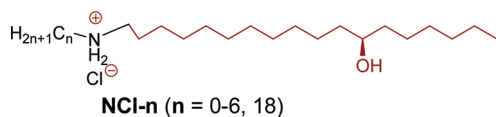
Although an enormous amount of effort has been made to identify and understand those features, they remain elusive.⁶ Progress is still limited by a general inability to determine the packing of molecules within their fibrillar networks. The number of single-crystal derived packing structures of gelators is small, and due to their frequent polymorphic nature, the number of those structures that can be related directly to the packing modes in the fibrillar networks of gels is even smaller. Unless new instrumental methodologies that allow access to molecular packing within a large number of fibrillar networks of gels are discovered, scientists will have to rely on a variety of techniques to link gelator structure to gel properties. Furthermore, to understand the factors that lead to efficient gelation, it is necessary to be able to compare the effects of small changes in gelator structure on gel structure and properties; the structures and properties of gels of several closely related gelators must be compared.⁷

Received: July 27, 2011

Revised: August 29, 2011

Published: October 06, 2011

Here, we provide such information, the “anatomy” of a series of molecular gels, in terms of their structures and dynamic properties, even though the insights derived from single-crystal packing are lacking. The molecular gelators investigated here are ammonium chloride salts derived from (*R*)-12-hydroxyoctadecanoic acid (HSA), *N*-alkyl-(*R*)-12-hydroxyoctadecylammonium chlorides ($\text{NCl-}n$, where the *n*-alkyl chain lengths, *n*, have 0–6 or 18 carbon atoms). Several of them are “ambidextrous”, gelating both water (a high-polarity, H-bonding liquid) and organic liquids, such as toluene and carbon tetrachloride (very low-polarity, aprotic liquids), and are very efficient (requiring <1 wt % concentrations to make gels at ambient temperatures). In addition, most of the $\text{NCl-}n$ gels are stable for months when kept in sealed containers (to avoid liquid evaporation) at ambient temperatures. Because the $\text{NCl-}n$ salts are the simplest ambidextrous gelators of which we are aware, they are very attractive to construct structure–gelator correlations. Thus, relationships between the structures and properties of the $\text{NCl-}n$ and those of their gels have been used to identify the salient features needed for gelators of this class to gel water or an organic liquid efficiently. In addition, detailed comparisons of the self-assembled fibrillar networks of the hydro- and organo-gels have been made at several length scales to investigate the manner in which the liquid molecules influence the eventual form of the fiber components.



■ EXPERIMENTAL METHODS

Details of materials preparations, instrumentation, and several procedures are described in the Supporting Information.

“Fast-cooled” gels were prepared by heating a mixture of the gelator and solvent (in a sealed glass tube, ~5 mm i.d.) until a solution/sol was obtained and then placing the tube directly into an ice–water bath (ca. 5–10 °C) for 10 min. Thereafter, the tube was kept at 23–24 °C for 1 h, and its appearance was noted. The procedure for preparation of “slow-cooled” gels was the same as above except that the hot sols were kept in their water or oil bath while it returned slowly to room temperature over a period of ~3 h. Unless stated otherwise, all gels were prepared by the fast-cooling protocol.

X-ray diffraction (XRD) studies were performed on a Rigaku R-AXIS image plate system with Cu $\text{K}\alpha$ X-rays ($\lambda = 1.54 \text{ \AA}$) generated by a Rigaku generator (46 kV and 40 mA). Data processing and analyses were performed using Materials Data JADE (version 5.0.35) XRD pattern processing software. Samples were sealed in 0.5 mm glass capillaries (W. Müller, Schönwalde, Germany), and diffraction data were collected for 90 min for the neat fibrillar networks and 10 h for the solvents and gel samples. The diffractograms of the solvents have been subtracted empirically from those of the gels to observe the reflections from the fibrillar networks.⁸

Small-angle neutron scattering (SANS) experiments were conducted at the Center for Neutron Research at the National Institute of Standards and Technology (NIST, Gaithersburg, MD, USA) using a NG7 30 m instrument⁹ over a set of three distances (15, 6, and 1 m) at a wavelength of $\lambda = 6 \text{ \AA}$, providing an overlap between the three configurations and, at the end, a range of scattering vector Q from 0.004 to 0.45 \AA^{-1} with ~ 250 useful

points in the range. Radial averaging of the isotropic 2D arrays was performed using the NIST software package.¹⁰ Specialized analyses were performed following the guidelines described in the field of molecular gels¹¹ and using other simple software. Cryo-SEM imaging was accomplished on a Hitachi S-4800 cold field-emission scanning electron microscope (SEM). A sample was plunged rapidly into slushed liquid nitrogen, followed by freeze-fracturing using the flat edge of a cold (-130°C) knife and then sublimation for 5 min at -95°C to etch away surface liquid and expose internal features. The sample was then sputter-coated with gold–palladium at 10 mA for 88 s. Detailed descriptions of SANS and cryo-SEM procedures are in the Supporting Information.

■ RESULTS AND DISCUSSION

Molecular design. Our efforts in this area have focused on a “bottom-up” approach in which we have started with structurally simple gelators, especially derivatives of long-chained *n*-alkanes, and modified them systematically and incrementally.^{1e} Recently, we explored in detail the gelating properties of amides and amines derived from the known efficient gelator,¹² HSA.¹³ HSA can be viewed as an *n*-alkane with substituents at a chain end (a carboxylic acid group) and along the chain (a hydroxy group) and, as such, a platform for the facile introduction of incremental structural changes. Because the analogous acid without the 12-hydroxy substituent, octadecanoic acid,¹⁴ and its amide and amine derivatives¹³ are much less efficient gelators than the corresponding ones derived from HSA, H-bonding involving the hydroxy groups is an integral contributor to the formation and stability of the fibrillar networks responsible for gel formation.¹⁵ Although several of the HSA-derived amides are exceedingly efficient gelators of organic liquids, some better gelators than the parent acid or its carboxylate salts,^{12d,15d,16} the corresponding amines are much less effective, and none is “ambidextrous”. As noted, addition of HCl to the amines transforms them into the $\text{NCl-}n$ salts, several of which are both ambidextrous and very efficient gelators.

The structural features of the $\text{NCl-}n$ homologues contain clearly identifiable sites that are amenable to stabilizing solvation by water (the 12-hydroxy group, the cationic ammonium center, and the anionic chloride) and by low-polarity organic liquids (the long octadecyl chain of the parent amine and the *N*-alkyl chain). However, to understand fully why some of the $\text{NCl-}n$ gelate a liquid but others of them do not, it is necessary to know the way in which the molecules pack within their aggregates and how that packing depends on the kinetics of their growth at different length scales. Although the final packing modes can be discerned from available analytical methods, the details of the kinetics of their growth remain enigmatic in the vast majority of cases studied.¹⁷ Thus, we concentrate here on the structural aspects of the gelators and their gels, although some kinetic data are provided.

Gelation Properties. “Ambidextrous” gelators, molecules that can gelate both water and organic liquids,¹⁸ are relatively rare, and those that require <1 wt % to make gels with *both* water and organic liquids are exceedingly rare. Although almost all known ambidextrous gelators have two distinct structural features—a hydrophilic part and a hydrophobic chain—many molecules with those features are not ambidextrous or even gelators of any common liquids. In fact, very few reports of truly ambidextrous gelators are found in the literature; in many examples, a gelator must be dissolved first in an organic (or aqueous) liquid before

Table 1. Appearances,^a T_{gel} Values ($^{\circ}\text{C}$),^b Representative Critical Gelator Concentrations (CGCs; wt % in brackets),^c Periods of Stability (in parentheses)^d of Gels Containing ~ 2 wt % NCl-*n* in Various Liquids (ordered by dielectric constants at 20 or 25°C)²⁰

liquid/gelator	NCl-0	NCl-1	NCl-2	NCl-3	NCl-4	NCl-5	NCl-6	NCl-18
water (80.1)	visc soln	visc soln	OG (57, >1 y) [0.3]	OG (76–77, >1 y) [0.3]	OG (83, >9 m) [0.3]	OG (94, >9 m) [0.3]	P	P
acetone/toluene (37.5)	P	P	OG (73–74, 8 m)	OG (76 ^e , >1 y) [0.4]	OG (67, >9 m)	OG (78–79, >9 m) [0.4]	OG (71–72, >9 m) [0.4]	P
methanol (32.7)	soln	soln	soln	soln	soln	soln	soln	OG (32–34, >1 y)
1-butanol (17.5)	soln	soln	soln	soln	soln	soln	soln	TG (34–35, 1 m)
benzyl alcohol (13.0)	soln	soln	soln	soln	soln	soln	soln	CG (33–35, 1 m)
1-octanol (10.3)	visc soln	P	P	P	P	TG (29–32, >9 m) [2.0]	TG (28–29, >9 m) [1.9]	TG (40–43, >1 y m) [0.9]
toluene (2.4)	soln	CG (syn, 74–75, >1 y) [0.5]	CG (77–78, >1 y) [0.5]	CG (74, >9 m) [0.5]	CG (72–73, >9 m) [0.5]	CG (68–69, >9 m) [0.5]	CG (60, >1 y) [0.5]	CG (60, >1 y) [0.5]
CCL ₄ (2.2)	visc soln	TG (76, >1 y) ^f	TG (76–77, >1 y) ^f	TG (76–77, >1 y) ^f [0.5]	TG (73, >9 m)	TG (72, >9 m) [0.5]	TG (69, >9 m) [0.5]	TG ^g (55, >1 y) [1.7]
<i>n</i> -dodecane (2.0)	P	P	P	I	I	I	P	visc soln
cyclohexane (2.0)	I	P	P	P	P	P	P	OG (70–71, >1 y)
<i>n</i> -hexane (1.9)	I	I	I	I	I	I	I	OG (83 ^d , >1 y) [1.8]

^a OG, opaque gel; syn, syndesis; soln, solution; visc, viscous; P, precipitated from sol; I, insoluble when heated in liquid; TG, translucent gel; CG, clear gel; y, year; m, month. ^b Temperature ranges between when the initial and final portions of an inverted gel sample fell on being heated slowly. ^c CGCs were determined from a series of fast-cooled gels with different fibrillar network concentrations; the concentration of the one with the lowest gelator concentration that did not fall when inverted at 24°C is reported. ^d Time between when a gel was prepared in a sealed container and when it underwent visually detectable phase separation after being kept at $\sim 24^{\circ}\text{C}$. ^e Phase separation observed. ^f Syneresis after 5 m. ^g Gel formed from sol after ~ 1 week at 22°C .

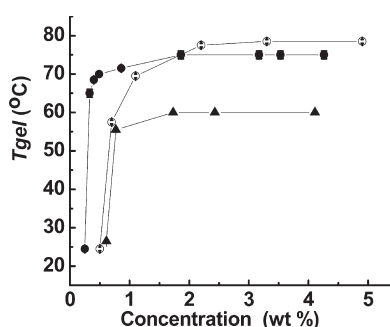


Figure 1. T_{gel} values as a function of concentration of NCl-3 in toluene gels (○), NCl-3 in hydrogels (●), and NCl-18 in toluene gels (▲). Vertical bars refer to temperature ranges over which the initial and final portions of a gel fell on being heated slowly; the absence of a space bar indicates that the range was smaller than the symbol.

adding it to water (or an organic liquid) to make a hydrogel (or organogel).

That procedure, but without the need for heating and cooling,¹⁹ could be used here, as well, to prepare some gels from the ambidextrous gelators (Supporting Information Table S1). For example, gels of NCl-3 were prepared almost instantaneously by adding water (a liquid in which the gelator is only slightly soluble) to solutions/sols in absolute ethanol (a liquid that is miscible with water and in which the gelator is much more soluble); the critical gelator concentration (CGC; defined experimentally as the smallest amount of gelator needed to keep a liquid from falling when the sample is inverted in a tube at 24°C) was ~ 0.7 wt % with 1/4 (wt/wt) ethanol/water as the liquid.

More importantly, both organo- and hydrogels of several of the NCl-*n* could be prepared directly from their sols, without addition of any cosolvent. A survey of the gelating abilities of the NCl-*n* salts and some basic properties of their gels, including representative CGCs, are presented in Table 1.

The liquids tested for gelation of the NCl-*n* include aromatics, H-bond donors and acceptors, and those with high and low dielectric constants.²⁰ Most of the data has been taken from samples at 2 wt % of gelator, in which, on the basis of the melting curves in Figure 1, the fibrillar networks are at or near their fully developed state. As noted in Table 1, the CGCs of several of the NCl-*n* hydrogels (*n* = 2–5), toluene gels (*n* = 1–6, 18), and acetonitrile gels (*n* = 3, 5, 6) are well below 1 wt %. Thus, the NCl-*n* are able to form gels in water and a wide range of organic liquids, and are able to do so at very low concentrations. In addition, the CGCs for gels of NCl-3 are 0.3 wt % in water and 0.5 wt % in toluene, whereas the T_{gel} values in the “plateau” concentration region (ca. 2–5 wt %) are ~ 75 and $\sim 78^{\circ}\text{C}$, respectively. The CGC of NCl-18 in toluene is slightly higher, 0.5 wt %, and the T_{gel} value in the “plateau” concentration region, $\sim 60^{\circ}\text{C}$, is somewhat lower than for the toluene gels of NCl-3. These differences can be ascribed, at least in part, to the higher solubility of NCl-18 than NCl-3 in toluene.

Viscoelastic Properties. As a representative example, we have investigated the rheological properties of gels of 2.1 wt % NCl-3 in water and toluene. At 25°C and 1 rad/s, the upper limit of the linear viscoelastic regime was $\sim 0.5\%$ strain in water and $\sim 0.2\%$ in toluene (Figure 2A). The values found in Figure 2 were reproducible to $\pm 2\%$ upon repetition of the experiments with the same sample. At higher strain percent, both the hydro- and organo-gel underwent phase separation. The viscoelasticity of these gels is demonstrated by the independence of the storage

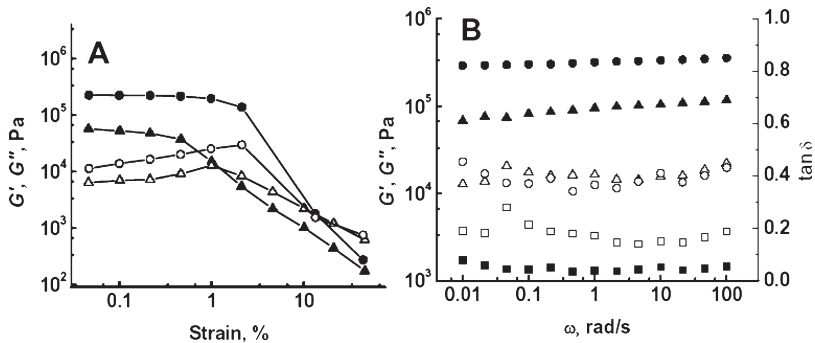


Figure 2. G' (filled circles or filled triangles) and G'' (open circles or open triangles) from log–log strain (A; 1.0 rad/s) and frequency (B; 0.1% strain) sweeps for a 2.1 wt % NCl-3 hydrogel (●) and toluene gel (▲) at 25 °C. (B) also shows $\tan \delta$ of the hydro (□) and (■) toluene gels.

(G') and loss (G'') moduli values over a range of applied frequencies of at least 0.01–100 rad/s at 25 °C and 0.1% strain (Figure 2B). At 25 °C and 2.1 wt % NCl-3, the hydrogel is mechanically stronger than the toluene gel: the value of the loss tangent, $\tan \delta = G''/G'$ (a measure of the strength of a viscoelastic substance²¹), is lower, and the yield strain limit is higher for the hydrogel ($\tan \delta = 0.05 \pm 0.01$; strain = 0.5%; $G' = 3.2 \times 10^5$ Pa, $G'' = 7.0 \times 10^4$ Pa) than for the toluene gel ($\tan \delta = 0.18 \pm 0.04$; strain = 0.2%; $G' = 9.3 \times 10^4$ Pa, $G'' = 1.6 \times 10^4$ Pa).

Hydrogels. Two weight percent of NCl-0 (i.e., the primary ammonium salt), NCl-1 (with an *N*-methyl group), and the NCl-*n* with the longest *N*-alkyl groups (i.e., NCl-6 and NCl-18) do not form hydrogels for different reasons. The sols of the relatively hydrophilic NCl-0 and NCl-1 remain dissolved in water at room temperature, and their aggregates are unable to form a supramolecular network at <5 wt %.^{22,23} The lower solubility (higher hydrophobicity) in water of NCl-6 and NCl-18 favors 3-dimensional nucleation and growth into bulk solids at the expense of 1-dimensional nucleation and growth needed for fiber formation. However, upon cooling aqueous sols of the NCl-*n* with *n* = 2–5, opaque hydrogels are formed. A similar dependence on the balance between hydrophilic and hydrophobic character has been reported for glutamate bolamphiphiles, whose sols in methanol/water mixtures lead to gels when the linker is butylene or pentylene and to a precipitate when the linker is hexylene.²⁴ Thus, the balance between solubility and insolubility of the NCl-*n* in water as well as the interaction energies of the aggregates and the rates of cooling determine the rates and modes of phase separation in the sols. As expected, the hydrogels are not stable in a strong base (where the NCl-*n* are reconverted to their amine precursors), but are stable in strong acid, at least at ambient temperatures. See the Supporting Information for details.

Organogels. The discussion here pertains to 2 wt % samples, selected to be at or near the plateau region of T_{gel} vs concentration curves (Figure 3). NCl-*n* with *n* = 0–6 produced only clear solutions/sols in polar, protic organic liquids such as methanol and 1-butanol. In the more lipophilic liquid, 1-octanol, only those gelators with longer *N*-alkyl groups—NCl-5, NCl-6, and NCl-18—formed (translucent) gels. In nonprotic, low-polarity liquids, such as CCl₄ and toluene, NCl-0 remained dissolved but NCl-*n* (*n* = 1–6, 18) formed translucent (in CCl₄) or transparent (in toluene) gels; only NCl-18 was able to gelate the least polar liquids, *n*-hexane and cyclohexane. In acetonitrile, a nonprotic liquid of polarity between that of water and CCl₄ or toluene, opaque gels were obtained only when the NCl-*n* with intermediate length *N*-alkyl chains, *n* = 2–6, were employed.

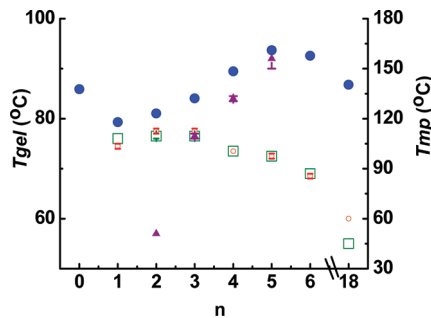


Figure 3. The dependence of melting points (T_{mp}) of neat NCl-*n* (●) and T_{gel} values of their 2 wt % gels with water (▲), CCl₄ (□), and toluene (○) by the falling drop method on *n*. Note that T_{gel} data points overlap for the CCl₄ and toluene gels of NCl-3, NCl-4, and NCl-5 (Table 1). If no data point is shown, the salt either remained soluble in or precipitated from the liquid.

These results emphasize the point made above, that liquid polarity and gelator hydrophilicity/lipophilicity are not the exclusive factors that determine whether a gel will form or how stable it will be;²⁵ the manner in which the phase separation from a sol phase occurs,¹ whether it prefers to lead to bulk crystals or a fibrillar network and the temporal stability of that network, must be considered, as well.

Melting Temperatures and NCl-*n* Structures. The vast majority of the aggregates here are spherulitic; some examples are shown in Figure 4. The constituent fibers are crystalline (vide infra), as in many other gel systems²⁶ and nucleating solutions.²⁷ The kinetics of nucleation, branching, and strength of molecular gels can be altered significantly by changing the thermodynamic driving force (i.e., changing the cooling rate or incubation temperature below the T_{gel} at which a sol is allowed to transform into a gel).^{17e,f,28,29} More highly branched fibrillar networks result when $T_{\text{gel}} - T_{\text{in}}$ is large (i.e., the incubation temperature, T_{in} , is low, and the driving force for phase separation in the supersaturated sol phase is large).^{2,17,30} These results have been explained on the basis of the interplay of rates of the various aggregation, nucleation, and growth processes that must accompany the transformation of gelators to their fibrillar networks. An example of this interplay is shown in Supporting Information Figure S3 for a very dilute (0.5 wt %) sample of NCl-3 in water ($T_{\text{gel}} \sim 67$ °C). The gel prepared by fast cooling contains very small, highly branched, spherulitic aggregates, and that from slow-cooling consists of larger, unbranched (non-spherulitic) bundles of fibers. A mixture of the two shapes is obtained from incubation at

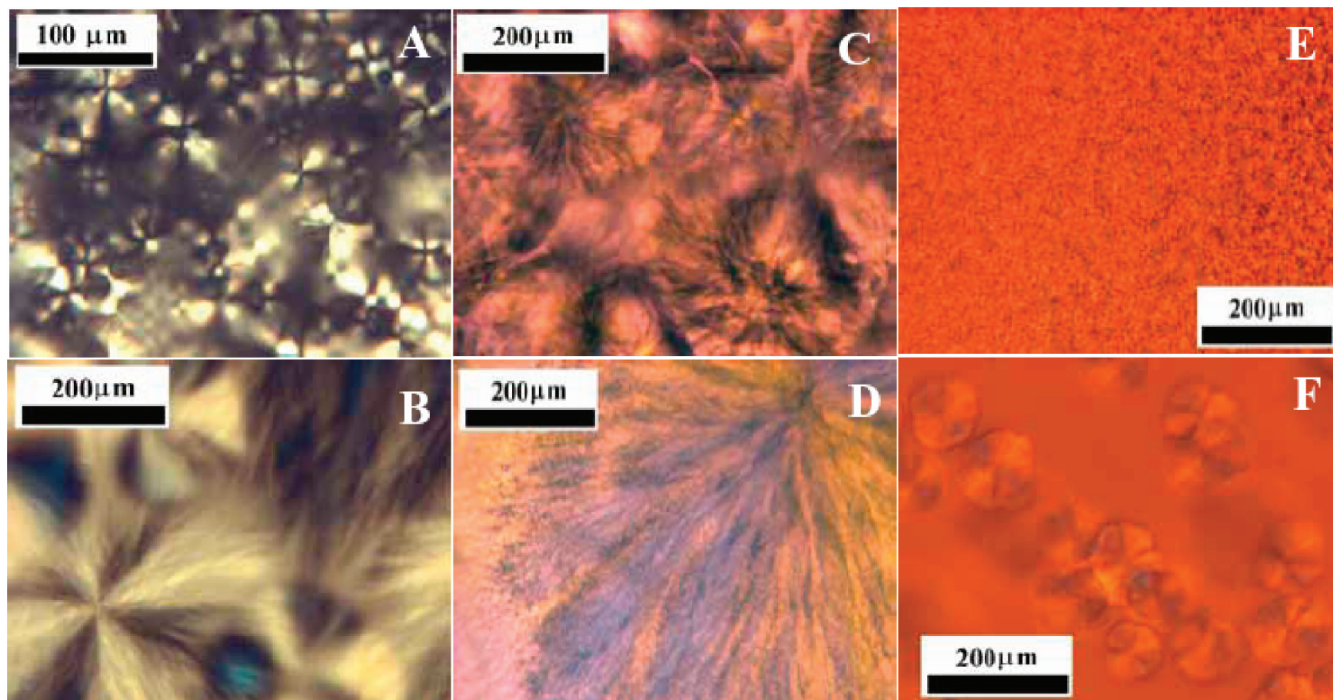


Figure 4. Polarizing optical micrographs at 23 °C of gels of 4.9 wt % NCl-3 in toluene (A, B), 4.8 wt % NCl-3 in water (C, D) and 1.9 wt % NCl-18 in 1-octanol (E, F) prepared by fast-cooling (A, C, and E) or slow-cooling (B, D, and F) protocols. The C, D, E, and F images were recorded with a full-wave plate.

50 °C, whereas the assembly from incubation at 62 °C is only rodlike.

Despite the differences between the fibrillar networks, the T_{gel} values of a selection of 2.0 wt % NCl- n hydrogels and toluene gels prepared by the fast- and slow-cooling protocols were found to be the same within experimental error. What is most striking about the data in Figure 3 is that T_{gel} values of the NCl- n ($n = 2–5$) hydrogels correlate with the melting temperatures, T_{mp} , of the neat solids, whereas the T_{gel} values of the organogels do not. We conjecture that the T_{gel} (hydrogel)/ T_{mp} correlation may be attributed in part to two important factors:³¹ (1) the solubility of the NCl- n in water must decrease somewhat (while the solubility in organic liquids increases) as n increases; and (2) XRD diffractograms (Figure 5 and Supporting Information Figure S4) demonstrate that molecular packing in the neat solids of NCl- n ($n = 2–4$, but not of NCl-5) and in their hydrogels is the same, whereas the molecular packing within the fibrillar networks of their organogels is different.

Thermodynamic Properties. From DSC thermograms, the normalized enthalpies for the gel–sol and sol–gel transitions, expressed as heat per gram of gelator (Supporting Information Table S2), and the temperatures of maximum heat flow at the transitions, T_{max} (near the mean melting temperatures for the fibrillar networks), have been calculated for NCl- n ($n = 2–5$) hydrogels and ($n = 2–4, 6, 18$) toluene gels. The precipitous increases in T_{gel} of the hydrogels as the concentrations of the NCl- n are increased and the fibrillar networks become more fully formed (see, for example, data for NCl-3 in Figure 6 and Supporting Information Table S3) were expected on the basis of the very low CGCs. The lower-temperature heating endotherm peaks in Figure 6 are from gel-to-gel transitions within the fibrillar networks.³² The XRD data in Figure 5A support our

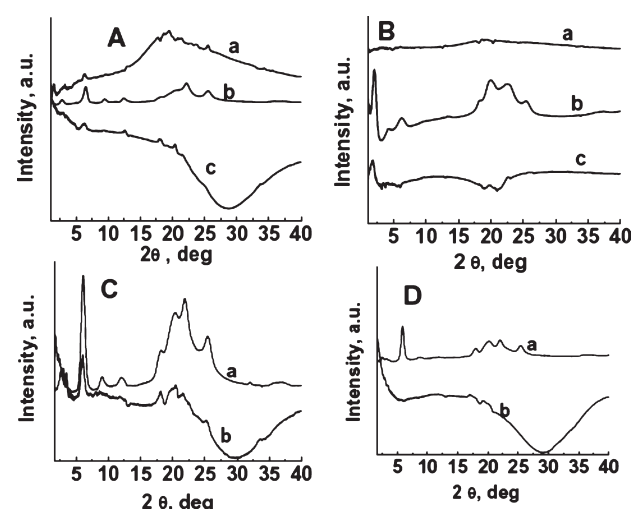


Figure 5. Vertically offset XRD diffractograms of NCl- n gels (after empirical subtraction of solvent diffractions) and of neat NCl- n powder at 22 °C: (A) 5.0 wt % NCl-3 in toluene gels (a), neat NCl-3 powder (b), and 5.1 wt % NCl-3 hydrogel (c); (B) 4.9 wt % NCl-18 in toluene gel (a), neat NCl-18 powder (b), and 4.9 wt % NCl-18 in 1-octanol gel (c); (C) Neat NCl-4 powder (a) and 5.0 wt % NCl-4 hydrogel (b); (D) Neat NCl-5 powder (a) and 5.1 wt % NCl-5 hydrogel (b).

contention that the transitions are not the result of separate melting of two coexisting morphs.³³

The heats of melting of neat NCl- n s and of the fibrillar networks in their gels can be compared directly only when the molecular packing arrangements are the same. Thus, the heats of melting of neat NCl-2 and NCl-3 and the normalized values for

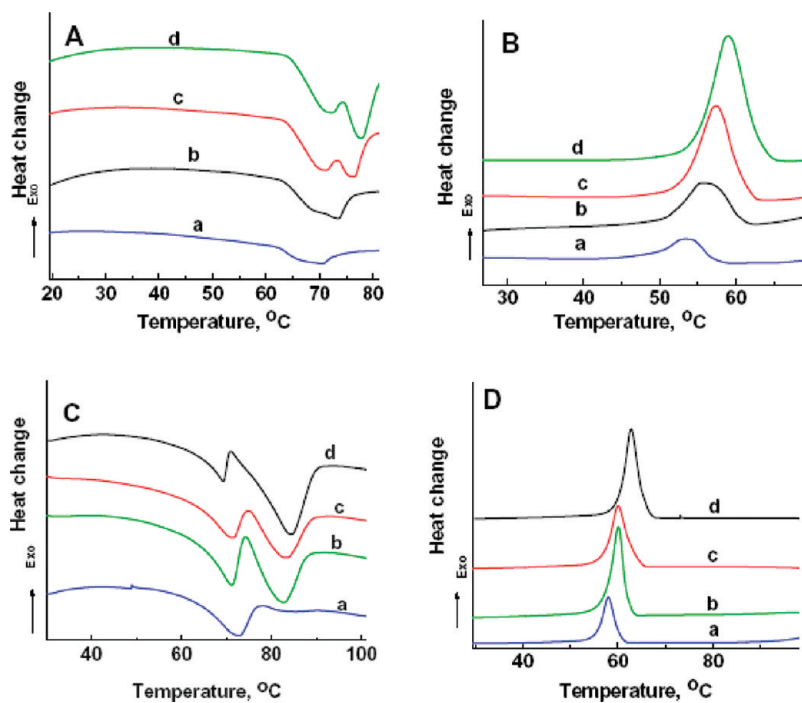


Figure 6. DSC thermograms for NCl-3 hydrogels (A and B) and toluene gels (C and D) during the second heating (A and C) and cooling (B and D) cycles. NCl-3 concentrations are (a) 0.7, (b) 0.9, (c) 1.9, and (d) 2.8 wt % for hydrogels and (a) 2.0, (b) 2.8, (c) 3.6, and (d) 4.9 wt % for toluene gels. See text for an explanation of the second heating endotherm.

their hydrogels, which share the same morph, are similar.³⁴ The molecular packing arrangements in neat NCl-2, NCl-3, and NCl-4 and in the fibers of their lower-temperature hydrogel phases are the same (but not for NCl-5 and NCl-18 at room temperature). The normalized ΔH values of the hydrogels of NCl-4 and NCl-5 are much larger than the heats of melting of the neat salts. The lower solubility in water of these gelators than their shorter homologues may be responsible for the disparity, especially if the heat of mixing of crystalline NCl-4 or NCl-5 into a liquid consisting of the same molecules (i.e., melting the neat solid) is lower than that needed to dissolve them into water.

Crystallinity and Molecular Packing within the Fibrillar Networks. X-ray diffraction peaks of the fibrillar networks of hydrogels with ~ 5 wt % NCl-*n* (*n* = 2–5) could be detected after empirical subtraction of the very large, broad, amorphous diffraction from water.⁶ Because the positions of the peaks from the neat powders (obtained by recrystallization from ethyl acetate solutions) and the hydrogel networks for NCl-*n* (*n* = 2–4) correspond to the same Bragg distances (Figures 5Ab, c, 5Ca, b and Supporting Information Figure S4), the molecular packing arrangements appear to be the same.³⁵ Furthermore, the broader diffraction peaks of hydrogels of NCl-5 (than those of the hydrogels of NCl-4, for example) suggest that its fibers are less crystalline.

The Bragg lattice spacings (*d*, Å) of the morphs of the NCl-*n* (*n* = 2–4) reported in Supporting Information Table S4³⁶ are based upon the lowest angle peaks in the diffractograms of the neat and hydrogel phases. Because they are very near the calculated extended molecular lengths,³⁷ the molecules may be arranged in layers, with the long axes of neighboring molecules either antiparallel (Figure 7A) or parallel (Figure 7B) and nearly orthogonal to the layer planes. Of the two, B is the less likely packing arrangement because molecules in adjacent layers must

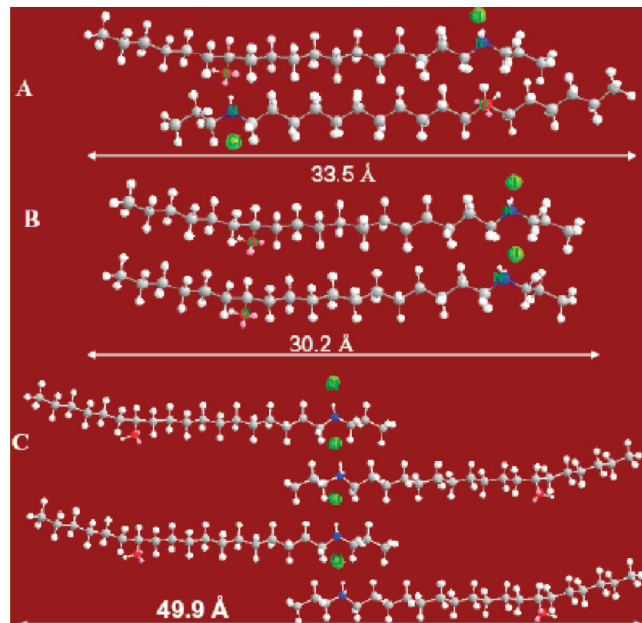


Figure 7. Two possible packing arrangements of molecules of NCl-*n* (*n* = 2–4) in hydrogel fibers (A and B) and one possible packing arrangement in fibers of NCl-3 in toluene gels (C) based upon XRD data and molecular mechanics 2 (MM2) calculations.

be parallel (i.e., a head-to-tail interlayer orientation); were the molecules in adjacent layers antiparallel, the calculated *d* spacing should be nearly twice the length of a molecule of NCl-*n*. In either case, the disparities between the calculated extended molecular length and the layer spacings may arise from bending

of the chains or their being aligned at a nonorthogonal angle to the layer planes, as indicated especially in Figure 7A.

The positions of the diffraction peaks of the fibers in the organogels examined³⁵ did not match those of the neat powders (Figure 5Aa, 5Ba,c), indicating different molecular packing arrangements within the fibers and the neat solids. For example, the Bragg distance for the sharp, lowest-angle peak of the 5.0 wt % NCl-3 in toluene gel is 55.2 Å, and the progression of peaks corresponds to distances of 27.5 and 13.8 Å (i.e., 1:1/2:1/3 ratios), supporting a layered packing arrangement. The 55.2 Å distance is somewhat shorter than twice the calculated extended length of an NCl-3 molecule, but significantly longer than the length of one molecule. For that reason, we conjecture that the molecules in the fibers are in bilayered arrangements similar to that shown in Figure 7C.³⁵ However, the calculated thickness of this bilayer is smaller than the Bragg distance corresponding to the lowest-angle peak, suggesting that less interdigitation than is shown may be possible, especially considering that the spaces between the long chains shown in the 2D cutaway would lead to gauche bends and additional shortening of the

bilayer thickness. Similar bilayer packing has been observed in other organogels.³⁸

The d spacings from the Bragg relationship of the peaks below 10° in 2θ in the diffractogram of neat NCl-18 (Figure 5Bb) are 42.8, 21.4, and 14.2 Å, corresponding to ratios of 1:1/2:1/3. These distances (and ratios), combined with the calculated extended length of a molecule of NCl-18, 49.9 Å³⁷ (Supporting Information Table S4), are again consistent with a layered packing arrangement. The diffractogram of an opaque gel of 4.9 wt % NCl-18 in 1-octanol exhibited a lowest-angle peak corresponding to a Bragg distance of 49.3 Å (Figure 5Bc), nearly the same as the calculated extended molecular length. Thus, the packing in the fibrillar networks of the 1-octanol gels may be layered, also, but must differ from the intraplane packing arrangement of the neat solid.

Comparison of the Fibrillar Network Structures of Organo-gels and Hydro-gels. Complementary structural information about the fibrillar networks at the nano-to-micro distance scales can be derived from analyses of direct space measurements (such as cryo-SEM) and reciprocal space measurements (such as SANS and X-ray diffraction). The selected cryo-SEM images of the fibrillar networks of a hydrogel and a toluene gel with low concentrations of NCl-3 at higher and lower magnifications in Figure 8 and Supporting Information Figures S7 and S8 are representative of the different structures found. The images demonstrate that fibers of the hydrogel are ~50 nm in width and twisted with a pitch ~120 nm (average of measurements on 10 fibers) (Figure 8A). The toluene gel structure consists of cylindrical (diameters ~55 nm; average of measurements on 10 fibers), and noncylindrical fibers of comparable dimensions (Figure 8C), both untwisted.

Figure 9A compares the SANS curves of aqueous and toluene gels of NCl-2. Striking differences appear in the whole Q range except at the lowest values (i.e., $Q < 0.01 \text{ \AA}^{-1}$, corresponding to the longest distance features in real space), where the scattering is nearly the same. These data suggest that the number density and contrast of the scatterers is similar and that the topography of the fibrillar networks is comparable at length scales $>600 \text{ \AA}$. A corollary conclusion is that the interaction modes of the resulting fibers in water or toluene are of comparable strength and induce the same type of “junction zones.” At this distance scale, the ionic character of the fibers connected in a fibrillar network does not

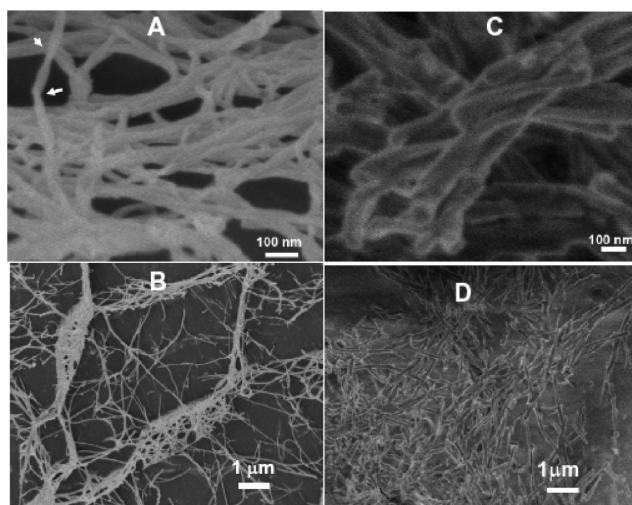


Figure 8. Cryo-SEM images of NCl-3 gels: (A and B) 0.5 wt % hydrogel, arrows indicate twists in a fiber; and (C and D) 1.0 wt % toluene gel.

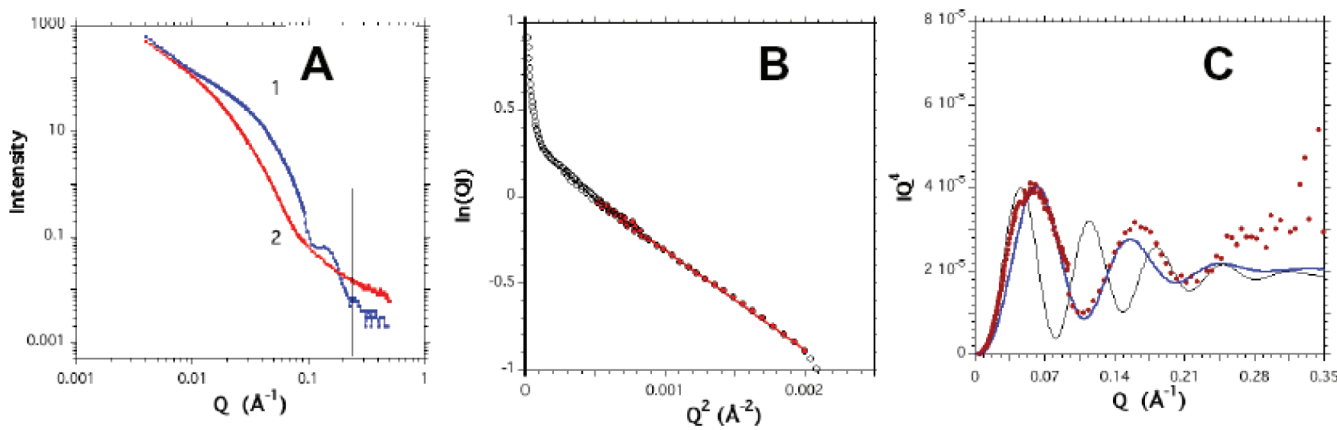


Figure 9. (A) SANS of 2.0 wt % NCl-2 in D_2O (1, blue dots) and in toluene- d_8 (2, red dots). The vertical bar is located at $Q = 0.24 \text{ \AA}^{-1}$. (B) Guinier's plot in which only full dots are used to find the best fit: $\ln(QI) = 0.2677 - 573.45Q^2$. Using eq 1, a value of the geometrical radius of the circular cross section, $R_0 = 47.9 \text{ \AA}$, is deduced. (C) Porod's plot in which full lines are theoretical adjustments to fit the red data points using eq 2: $R_0 = 48 \text{ \AA}$, $\epsilon = 0.10$ (gray); $R_0 = 36 \text{ \AA}$, $\epsilon = 0.15$ (blue).

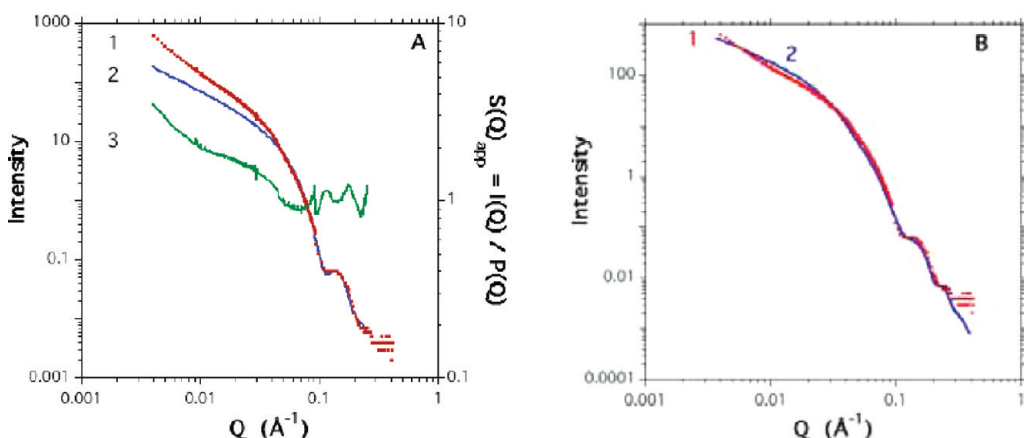


Figure 10. SANS of 2.0 wt % NCl-2 gel in D_2O : (A) (1) experimental data, (2) best fits according to eqs 2 and 3 with $R_0 = 36 \text{ \AA}$, $\varepsilon = 0.15$, and (3) $S(Q)_{\text{app}}$ obtained from eq 4, assuming $P(Q)$ is the scattering; (B) (1) experimental data and (2) fit according to modified eq 5 with $n_b = 6$.

generate a specific solidlike architecture. The following form-factor analysis clarifies the situation.

For $Q > 0.01 \text{ \AA}^{-1}$, the scattering curves are very different: in water, the profile of the intensity decay is shifted to larger Q values than in toluene, and two oscillations are present; in toluene, the decay is smooth to the longest Q investigated, $\sim 0.5 \text{ \AA}^{-1}$. The very different scattering curves indicate that (1) the NCl-2 gelator differentiates the polarity of the media, and (2) the balance among hydrophobic, ionic, and van der Waals interactions is responsible for the specificity of the aggregates and fibrillar networks only for $\langle d \rangle < 600 \text{ \AA}$.³⁹ The twisted fibers of the hydrogel and untwisted cylinders of the toluene gel seen in Figure 8 support the first point, that the interfacial energies experienced by the fibers in the two liquids are very different.⁴⁰ The observation that the second oscillation, at $Q = 0.24 \text{ \AA}^{-1}$, in the hydrogel coincides in Bragg space with the first diffraction peak observed in the X-ray diffractogram (Supporting Information File Table S4) suggests, but is insufficient to conclude unambiguously, that the fibers consist of layers of NCl-2 molecules.

As a first step in the form-factor analysis, we have determined whether a linear domain in a Guinier's plot, $\ln(QI)$ vs Q^2 , is present (Figure 9B). Note that the scattering curve in both gels deviates from the central linear slope on both the low- and high- Q sides; the scattering signatures of the internal molecular structure of the fibers and the structure factor of the fibers in "junction zones" can affect the high- and low- Q parts of the SANS curves, respectively. For this reason, we have constructed, as well, a Porod's plot, IQ^4 vs Q , for data in the high- Q region (Figure 9C). As mentioned, Figure 9C clearly shows the contribution of the "junction zones", appearing as an intense extra scattering in the lowest Q part of the curve, that is not taken into account in the linear fit. Using eq 1,¹¹ a value of the geometrical radius of the circular cross section, $R_0 = 47.9 \text{ \AA}$, can be calculated. The shape of Figure 9C demonstrates that this value provides a poorer fit to the data in a Porod's plot than does the modeling for thinner fibers, $R_0 = 36 \text{ \AA}$; as noted above, the contribution of the junction zones alters the Guinier's regime.

The second oscillation in Figure 9C appears as a form-factor oscillation. The slight deviation from the model curve (N. B., an excess of intensity) may be a consequence of the coincidental location of a Bragg peak. The spacing measured by X-ray diffraction can be attributed to periodic high electron density units. In NCl-2, this corresponds to the chloride anion associated

with the positively charged nitrogen atom. The scattering in SANS arises from the entire morphology, acting as a continuum of neutron scattering length density at the nanoscale with respect to the deuterated solvent.

$$QI = QI_0 \exp -Q^2 R_c^2 / 2 \approx QI_0 \left(1 - \frac{R_c^2}{2} Q^2 \right) \quad (1)$$

In eq 1, R_c is the cross-sectional radius of gyration (with $R = R_c(2)^{1/2}$). The other parameters are explained in the Supporting Information.

$$I = \frac{\pi C}{Q} \Delta b M_L \left[2 \frac{J_1(QR)}{QR} \right]^2 \quad (2)$$

In eq 2, C is the rod concentration (g cm^{-3}), M_L the mass per unit length of a rod (g \AA^{-1}), Δb its specific contrast ($\Delta b = b_2 - \rho_s v_2$), b_2 is the specific scattering length of a rod (cm g^{-1}), v_2 its specific volume ($\text{cm}^3 \text{ g}^{-1}$), ρ_s is the scattering length per unit volume of the solvent ($\text{cm} \text{ cm}^{-3}$), and R is the radius assuming a circular cross section. Equation 3 takes into account the radial polydispersity that modulates the diameter values (thermal fluctuations) as a convolution with a normalized Gaussian distribution function (full width $\Delta R_{1/2}$).

$$\varepsilon = \frac{\Delta R_{1/2}}{2R_0}, \quad X = \frac{R}{R_0} \quad (3)$$

$$QI \propto \frac{1}{\varepsilon} \sqrt{\frac{\ln 2}{\pi}} \int \left(\frac{2J_1(QR_0x)}{QR_0x} \right)^2 \exp -\frac{\ln 2}{\varepsilon^2} (x-1)^2 dx$$

To evaluate the importance of the junction zones in the hydrogel network, the theoretical form-factor scattering (as determined in Figure 9B) is compared with the experimental I vs Q curve (Figure 10). A significant difference between the two that can be assigned to the contribution of heterogeneities larger than the constituent fibers (diameter ca. 72 \AA) exists at $Q < 0.045 \text{ \AA}^{-1}$. At $Q > 0.045 \text{ \AA}^{-1}$, the agreement between the experimental and theoretical curves (including the second form-factor oscillation) is good. The shape of this extra contribution can be estimated by extracting an apparent structure factor $S(Q)_{\text{app}}$ following eq 4, assuming an average interaction potential between the fibers with a spherical symmetry. This procedure is reasonable because the

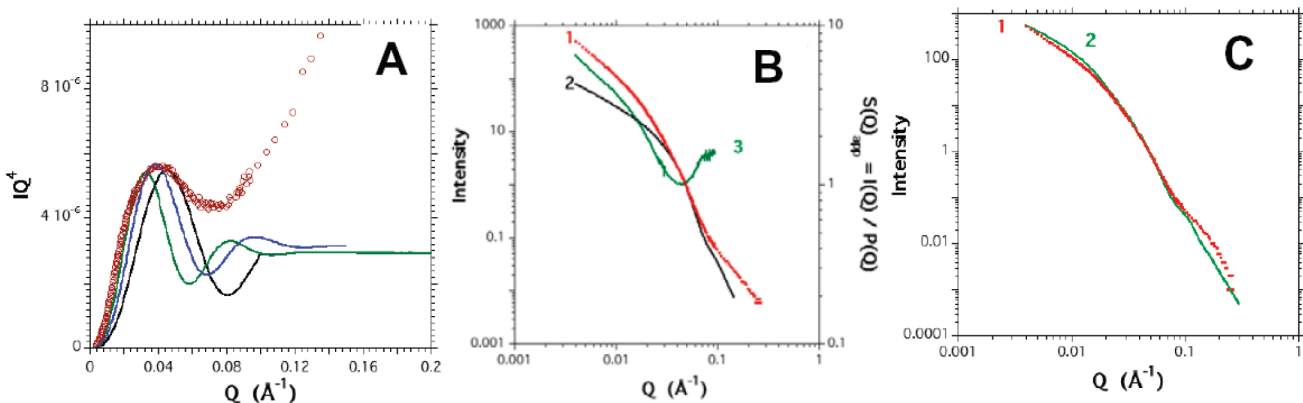


Figure 11. SANS of 2.0 wt % gel NCl-2 in toluene-*d*8. (A) Porod's plot. Dots are experimental data. Solid lines are theoretical adjustments following eqs 2 and 3 with $R_0 = 60 \text{ \AA}$ and $\varepsilon = 0.20$ (blue), $R_0 = 70 \text{ \AA}$ and $\varepsilon = 0.20$ (black), and $R_0 = 50 \text{ \AA}$ and $\varepsilon = 0.18$ (green). (B) Intensity-vs- Q plot of experimental data (red), best fit according to eqs 2 and 3 with $R_0 = 56 \text{ \AA}$ and $\varepsilon = 0.24$ (black), and $S(Q)_{\text{app}}$ obtained from eq 4 (green). (C) Experimental data (red dots) and theoretical model for a suspension of fibers ($R_0 = 56 \text{ \AA}$, $\varepsilon = 0.15$) and bundles according eq 5 with $n_b = 12$ (green).

scattering features characteristic of the form factor and their interactions are well separated in terms of Q values (eq 4).

Curve 3 in Figure 10A shows an enlargement of $S(Q)_{\text{app}}$. For $Q > 0.009 \text{ \AA}^{-1}$, the profile is comparable to that for the theoretical form factor of fibers, whereas for $Q < 0.009 \text{ \AA}^{-1}$, a kink indicates a change in the scattering regime: for $Q > 0.009 \text{ \AA}^{-1}$, it is reasonable to assume that bundles can be formed through juxtaposition of fibers whose form-factor contribution (eqs 2 and 3) corresponds to this part of the extra scattering, $S(Q)_{\text{app}}$. For $Q < 0.009 \text{ \AA}^{-1}$, the scattering intensity is assigned to other heterogeneities in the fibrillar network (opaque gels) contributing to enhanced amplitude.

$$S(Q)_{\text{app}} = I(Q)/P(Q) \quad (4)$$

Large-scale heterogeneities in fibrillar networks (e.g., flocs or spherulites)⁴¹ could be described through a random two-phase model (Debye–Bueche's model)⁴² in which correlations of heterogeneities are damped as an exponential decay, whereas in reciprocal space, the related intensity is a sharp Q^4 upturn. For reasons of simplicity, only one inhomogeneous bundling process, delivering longitudinally packed fibers, is considered to model the scattering at $Q > 0.009 \text{ \AA}^{-1}$ in Figure 10. The effective interaction of self-assembled, rodlike aggregates in semi-dilute solutions is complex, attractive, anisotropic, and salt-dependent.⁴³ Bundles may result from a balance of electrostatic forces and hydrophobic interactions, but it seems here, as in the vast majority of molecular gels, that there is no energy minimum, and only kinetic barriers limit the bundling process. Over time, the fibrillar networks are expected to phase-separate, illustrating the intrinsic metastability of molecular gels.

The bundles are assumed to be formed by close packing the cylindrical fibers ($R_0 = 36 \text{ \AA}$), resulting in a fiberlike envelope of radius B for which the form-factor scattering can be easily calculated. For a number, n_b , of single fibers in a bundle, the radius is $B = R_0(n_b)^{1/2}$. The scattering is assumed to be additive for all components (form-factor assumption) in the mixture from $n_b = 1$ ($B = R_0$) to n_b ($B = R_0(n_b)^{1/2}$). Equation 5 is accordingly used for each component; $w(n)$ is the volume weight of the population of bundles formed by n fibers, and $P(Q)$ is the form factor of a plain cylindrical fiber as defined in eqs 2 and 3. The choice of the weight, $w(n)$, for each population as well as that of the value n_b

need not be determined well for the qualitative conclusions, which are drawn here. Figure 10B shows the very satisfactory fit of a model for $n_b = 6$ (corresponding to a precursor situation for hexagonal arrangements frequently encountered in more concentrated systems⁴⁴) to the experimental data over the whole Q range. On the basis of these analyses, the 2 wt % NCl-2 hydrogel contains a fibrillar network with fibers interconnected through bundles involving 2–6 tightly packed, rigid fibers ($R_0 = 36 \text{ \AA}$) in approximately equal proportions.

$$I(Q) = \sum_{n=1}^{n_b} w(n) P(Q) \quad (5)$$

As noted, SANS data for the NCl-2 organogel are very different in many aspects from those of the hydrogel (see Figure 9). The scattering from the toluene gel does not display a linear domain in a Guinier's plot (not shown). Its absence confirms the very strong contribution of the “junction zones” on the form-factor scattering of the fibers. The high- Q domain (Porod's regime) of the scattering curve shows an oscillation (Figure 11A). Attempts to model this (vide infra) show that a range of diameters is necessary to account for its large width. Figure 11B shows that the fibers are thick ($R_0 = 56 \text{ \AA}$) and much more radially disperse than those in the hydrogel. The $S(Q)_{\text{app}}$ profile does not have a kink (as found in water), suggesting a more continuous and homogeneous bundling process in the fibrillar network of the toluene gel than in the hydrogel.

Figure 11C shows that the bundling mechanism can be accommodated by eq 5: the fibrillar network consists of a variable volume fraction of fibers of different diameters and in bundles with n_b as high as 12. This requirement for good fits to the data confirms the indications of a denser mesh of thicker fibers ($R_0 = 56 \text{ \AA}$ in toluene vs 36 \AA in water) but more homogeneous than in water because no Debye–Bueche scattering component can be detected.

The same general approach (i.e., utilizing a combination of the best fit of the constituent fibers obtained in the Porod's regime, the $S(Q)_{\text{app}}$ profile to determine the amplitude of the bundling and its “homogeneity”, and the modeling of the low- Q extra-scattering component as resulting from junction zones described by the “bundling model” of eq 5) can be used to analyze the other gels of the series. For example, $R_0 = 57 \text{ \AA}$, $n = 6$ and $R_0 = 65 \text{ \AA}$, $n = 3$ are obtained for 2 wt % hydrogels of NCl-3 and NCl-4,

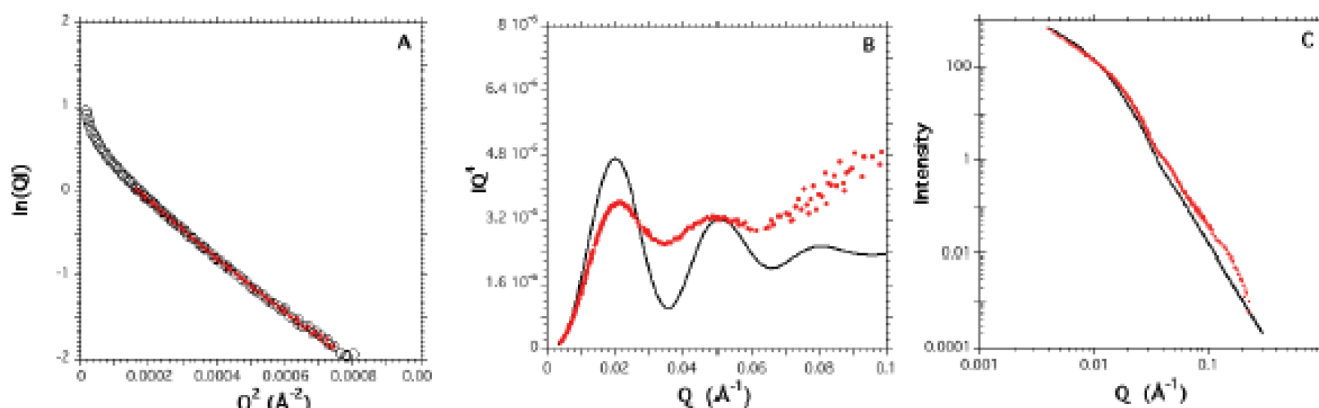


Figure 12. SANS of a 1.0 wt % NCl-18 gel in toluene- d_8 : (A) Guinier's fit, $\ln(QI) = 0.5284 - 3259.3Q^2$, $R_0 = 114.2 \text{ \AA}$ (red straight line), to experimental data (dots; only those in red are used to obtain the linear fit); (B) Porod's plot, IQ^4 vs Q : experimental data (red dots) and theoretical model using eq 1 with $R_0 = 110 \text{ \AA}$, $\varepsilon = 0.15$ (solid line); (C) fit to experimental data (red dots) according to eqs 2, 3, and 5 for $R_0 = 110 \text{ \AA}$, $\varepsilon = 0.18$, $n_b = 6$ (full line).

respectively (Supporting Information Figure S9). Thus, taken with the NCl-2 results, there is a clear trend that increasing the molecular length of the gelator increases the width of the fibers in their hydrogels. An irregular, less pronounced trend is observed in the corresponding toluene gels, in which the R_0 values at 2 wt % NCl-2, NCl-3, and NCl-4 are $R_0 = 56, 70$, and 65 \AA , respectively (Figure 11 and Supporting Information Figure S10). As noted above and based upon the XRD data, the packing of molecules within the toluene gels of these 3 gelators differs from one homologue to another; there is no reason, therefore, to expect a consistent trend in R_0 for their fibers.

Scattering from the toluene gel with 1.0 wt % NCl-18, the longest NCl- n , is mixed with a significant amount of “extra scattering” from bundles; a mean value of $R_0 = 110 \text{ \AA}$ was calculated using eqs 2 and 5. Although the diameter, $\sim 220 \text{ \AA}$, is comparable to the extended length of 4 to 5 NCl-18 molecules (49.9 \AA , see Supporting Information Table S4), insufficient information is in hand to conclude that the internal structure of the fibers consists of bilayers. On the basis of the analytical approach described above, the NCl-18/toluene gel consists of a statistical distribution of aggregated fibers ($2 < n < 6$) with a flat histogram of number density ($w(n) \approx 0.17, \forall n$) (Figure 12). Because the SANS curves result from scattering over a relatively large volume, $\sim 300 \text{ mm}^3$, the structural information describes the average situation, where thicker fibers or bundles dominate the scattering (proportional to the volume of specific scatterers).

Temporal Evolution of SANS Curves. In some cases, it was possible to observe the temporal evolution of the scattering curves (and, thus, some aspects of the formation of the fibers and the bundling process) when sols/solutions were incubated at temperatures below T_{gel} .

The choice of the acquisition (30 s) and interval (variable) times for these kinetic runs is a compromise between increasing signal intensity (longer collection times) and time resolution (shorter collection times). Figure 13A shows the series of scattering curves collected in the intermediate Q range (sample-detector distance = 6 m) for (initially) a sol of 2.0 wt % NCl-18 in toluene- d_8 incubated at 53 °C (i.e., no detectable signal) and ending in the gel state (i.e., an intense signal). When the intensity at Q_{\min} in this range is plotted versus time, a classical sigmoid curve (Figure 13B) is obtained, showing that the induction time, t_i , is ~ 300 s and the fibrillar growth is very fast ($\Delta t \approx 100$ s), but the equilibration time is much longer ($t_{\text{eq}} > 1000$ s).

Figure 13C is the Holzer's plots of the scattering data to follow the increasing number density of fibrillar aggregates as time increases. According to eqs 1 and 2, the low- Q asymptotic behavior is a Q^{-1} decay (a plateau in the Holzer's plot), and the extrapolated value at $Q \rightarrow 0$ is proportional to the volume of the scatterers, thereby relating also the ordinates of Figure 13B. The theoretical form-factor scattering for fibers with $R_0 = 95 \text{ \AA}$ and $\varepsilon = 0.18$ is also reported (vide infra) and reproduces well the experimental low- Q profiles.

A basic question concerning the kinetics of fibrillar growth in molecular gels is whether structural intermediates appear and disappear before the equilibrium fibrillar network morphology (in this case, cylinders with $R_0 \approx 110 \text{ \AA}$ for NCl-18 in toluene gels) is reached.

The above analysis has shown that because of bundling (either homogeneous or biphasic and random), the signal in the Guinier's domain is affected by an extra scattering component $S(Q)_{\text{app}}$ at the first stages of growth. As the process continues, increased metastability might occur at the final stages. Therefore, a clearer structural analysis employs the Porod's Q domain. Figure 14A shows the kinetic sequence of the corresponding Porod's plots for the data in Figure 13. At this stage and considering the poor quality of the statistics, the first form-factor oscillation seems to be centered at the same position during the first 300 s of the gelation process. No other population at a significant volume fraction or with a significantly different diameter value can be observed. Figure 14B reveals details of the location of the oscillation with respect to the position of an equilibrated gel: the oscillation shifts by 0.004 \AA^{-1} , from 0.0243 to 0.0203 \AA^{-1} . The above analysis has demonstrated that bundling generates a distribution of larger diameters (according to eq 5), but also induces a shift at large Q values. The actual diameter of the fibers can be approximated from the plots in Figure 14B, where the theoretical profile for $R_0 = 95 \text{ \AA}$ and $\varepsilon = 0.18$ is also plotted. Given the nature of the scattering curves collected over time, the agreement between these parameters and those calculated for the “equilibrated” gel is very good.

The analysis has thus allowed the identification of a bundling mechanism in the NCl- n fibrillar networks and the characterization of bimolecular associations (see Supporting Information Table S4) in the internal structure of the fibers. The bundling mechanism develops fully over time scales longer than the SANS collection times in Figure 14. As shown in various other

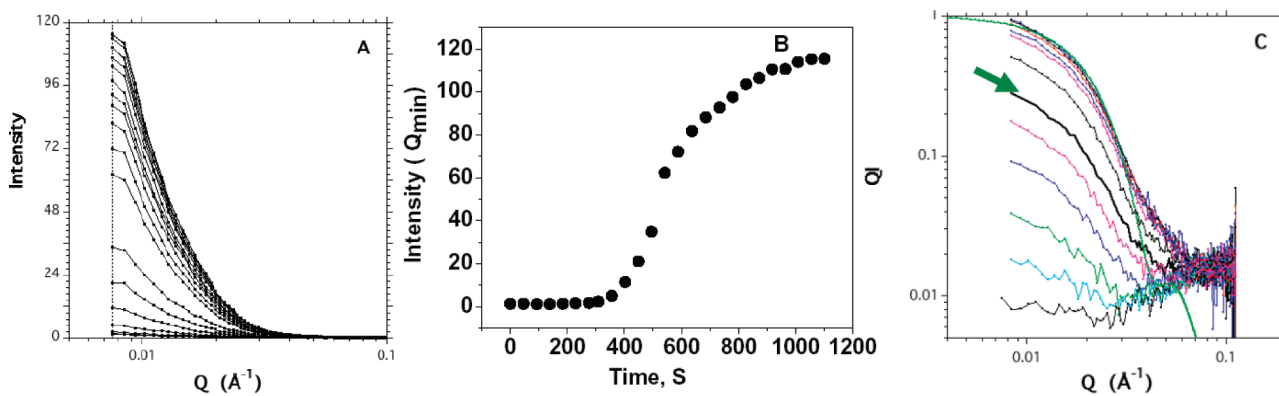


Figure 13. SANS kinetic data for 2.0 wt % NCl-18 gel in toluene- d_8 incubated at 53 °C: (A) I vs Q (solvent-corrected); (B) sigmoidal curve from plot of total intensity ($I(Q_{\min})$) vs time; (C) Holzer plots of data (QI vs Q). Note that part B correlates the temporal curves in parts A and C. The solid green line with an arrow is the theoretical form-factor scattering for $R_0 = 95 \text{ \AA}$ and $\varepsilon = 0.18$ according to eqs 2 and 3.

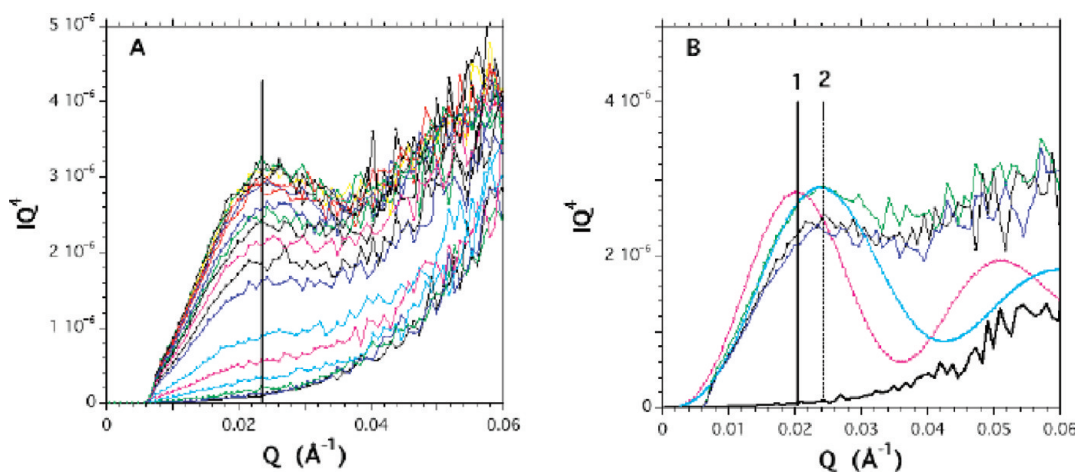


Figure 14. SANS kinetic plots for 2.0 wt % NCl-18 in toluene- d_8 incubated at 53 °C: (A) IQ^4 vs Q (solvent-corrected); (B) selection and theoretical scattering functions (full lines) using (1) $R_0 = 110 \text{ \AA}$, $\varepsilon = 0.15$ (full vertical points at the apex of the first theoretical oscillation) and (2) $R_0 = 95 \text{ \AA}$, $\varepsilon = 0.18$ (dotted vertical points at the apex of the first experimental oscillation).

molecular organogels investigated by SANS, bundling is frequently a first-order process.^{17g}

The intensity in Figure 13B is related to the degree of aggregation of NCl-18 in toluene and, thereby indirectly, to the amount of the gel network present at various times. Assuming that no aggregates of NCl-18 are present at time = 0 (time = 0 is taken to be the start of the inflection of the data in Figure 13B after the induction period) and that the aggregation and extent of fibrillar network formation are at their equilibrium values when the SANS intensities no longer increase perceptibly with time (i.e., at time operationally approaching ∞), the fraction of the gel phase at time = t , ϕ_g^t , can be expressed in terms of the intensities at time = 0, t , and ∞ ($I(0)$, $I(t)$, and $I(\infty)$, respectively): $\phi_g^t = (I(t) - I(0))/(I(\infty) - I(0))$.⁴⁵ Then, values of K are obtained most easily from single-exponential decay fits of the data using eq 6, and the Avrami exponent, n_A , is most easily extracted from eq 7 by plotting $\ln(-\ln(1 - \phi_g^t))$ vs $\ln t$ (Supporting Information Figure S11A). The value of n_A is a function of both the dimensionality of growth and the mode of nucleation (i.e., heterogeneous or instantaneous).^{2,46} From treatment of the data in Figure 13B according to eq 7, the value of n_A is calculated to be 1.94 ± 0.12 (Supporting Information Figure S11A). There are

two proposed possibilities when an Avrami constant is 2: (a) instantaneous nucleation to platelet-type objects or (b) heterogeneous nucleation to rodlike objects.⁴⁷ Because the aforementioned POM and cryo-SEM images and the SANS data are consistent with rods but not platelets within the gel networks, nucleation must be heterogeneous, occurring throughout the solution/sol to gel transformation.⁴⁸

$$1 - \phi_g^t = \exp(-Kt^n A) \quad (6)$$

$$\ln \left[-\ln \left(1 - \phi_g^t \right) \right] = n_A (\ln K + \ln t) \quad (7)$$

CONCLUSIONS

Although several other ambidextrous gelators have been reported previously,¹⁸ their molecular structures are more complex than those of the NCl- n , and detailed comparisons of their fibrillar networks in the organo-gels and hydrogels have not been made. In addition, we are unaware of other classes of ambidextrous gelators having molecular structures as simple as those of

the NCl-*n* that are able to gelate both water and many organic liquids at ~0.5 wt % concentrations. In general, the differences observed between organo-gels and hydrogels of the same NCl-*n* can be explained primarily on the basis of electrostatic effects. Coulombic interactions in the hydrogel are reduced by the permanent dipole moments of water molecules (i.e., a dielectric screening effect); in the organo-gels, screening, as indicated by the ratio of dielectric constants (for example, $\epsilon^{\text{DC}}(\text{H}_2\text{O})/\epsilon^{\text{DC}}(\text{toluene}) = 33.6$), is much less. Thus, in water, the system is dominated by hydrophobic interactions and long-ranged electrostatic repulsions, but in the lower-polarity organic liquids, the reduced ionization of the fibers does not counterbalance the van der Waals attractive component, leading to larger bundles.

In addition, kinetic data obtained from SANS measurements on a supercooled sol of NCl-18/toluene reveal additional important information about the mode of fibrillar growth leading to gelation. According to Avrami theory, heterogeneous (rather than spontaneous) nucleation leads to the rodlike objects observed. In other systems, the modes of growth were found to be heterogeneous (at higher incubation temperatures) and homogeneous (at lower incubation temperatures) nucleation for cholesteryl *N*-(2-naphthyl)carbamate/ethyl acetate gels and homogeneous nucleation throughout the temperature range explored for cholestanyl *N*-(2-naphthyl)carbamate/alkane gels.^{17e,f} As one would expect, one-dimensional fibrillar objects can be achieved by a variety of nucleation and growth mechanisms that depend on gelator structure, concentration, the liquid component, and temperature.

The self-aggregation properties of the NCl-*n* can be altered drastically by varying the *N*-alkyl chain length in ways that are explicable on the basis of polarity and size. Thus, addition of NCl-0 to water as well as to some organic liquids results in viscous solutions within the concentration range explored, but there is no evidence for formation of the entangled networks necessary for gelation. NCl-1, in which one of the hydrogen atoms on the nitrogen of NCl-0 has been replaced with a methyl group, forms organo-gels in CCl₄ and toluene, but it does not gelate water (where it remains solubilized). The NCl-*n* with somewhat longer methylene chains attached to nitrogen (*n* = 2–5) become ambidextrous; the balance between hydrophilic and lipophilic character, as well as the packing arrangements of these molecules, permit one-dimensional fibrillar growth in both aqueous and organic media, but the nature of the molecular packing within the fibers of the two types of gels is very different.

Finally, the NCl-*n* with the longest *N*-alkyl chains and highest lipophilicity, NCl-6 and NCl-18, are not ambidextrous and gelate only organic liquids. Thus, by adding or subtracting even one methylene of an *N*-alkyl group, the self-assembling process at the submicrometer to micrometer length scale (i.e., fibrillar, one-dimensional objects vs 2- or 3-dimensional crystallization or a lack of precipitation) can be controlled and understood primarily on the basis of solubility. Furthermore, the fibrillar growth appears to occur with the polar head groups of highly interdigitated bilayers (or tilted monolayers) directed toward the liquid interface in water and with the hydrophobic 12-hydroxyoctadecyl tails pointed toward the liquid interfaces and the charged centers near the middle of bilayer arrangements in the organogels. In each case, the molecular organization within the fibers minimizes interfacial energy. Individual fibers then bundle over time to reduce further their interfacial energy (i.e., a form of Ostwald ripening).

The data also indicate that as the length of the *N*-alkyl group increases, it becomes more difficult for the polar groups to be in sufficient proximity to the aqueous part of the hydrogels for one-dimensional growth; the layers in the fibers cease to form when the “screening effect” of long *N*-alkyl groups exceeds a limit. Similarly, the bilayered packing within the fibers of the organogel cannot be maintained beyond a certain *N*-alkyl chain length, but for very different reasons. In the bilayers, the space occupied by the *N*-alkyl groups must be appropriate to allow retention of the H-bonding network along the 12-hydroxyoctadecyl chain as well as a network of stabilizing electrostatic interactions at the polar head groups.⁴⁹ At lengths beyond a critical limit, one or both of these interactions become disrupted, and a different molecular packing arrangement occurs that is not conducive to fibrillar growth.

The bundling of twisted fibers of NCl-3 in its hydrogel and of cylindrical fibers in its toluene gel, seen in cryo-SEM images, has been quantified by careful analyses of SANS data. The latter also show that increasing the molecular length of the NCl-*n* increases the width of the fibers in their hydrogels (which may be a cause for the increasing values of T_{gel} as the *N*-alkyl chain lengths increase). However, no simple hypothesis can be advanced to explain the irregular, less pronounced trend in T_{gel} with increasing *N*-alkyl chain length in the organogels (N.B., data for toluene gels); although all of these fibers seem to be composed of NCl-*n* molecules in bilayers, the details of the subtle differences in how the *N*-alkyl groups affect packing within those layers and, thus, the electrostatic interactions of the head groups cannot be discerned with the information in hand. Such information is integral to analyzing the relationship between *N*-alkyl chain length and T_{gel} and in understanding why the hydrogel of NCl-3 is stronger mechanically than the corresponding toluene gel.

In summary, the results presented here demonstrate that the NCl-*n* are a versatile platform for interrogating fundamental questions regarding the links between molecular structure and one-dimensional self-aggregation leading to gelation. They lead to gels with a wide range of liquids and at very low concentrations. Their structures are amenable to several systematic variations that provide a matrix of information linking gelator structure and gel properties.

Future work will investigate how exchanging the Cl[−] anion for ones of different size and Lewis basicity influences the gelating ability of the (R)-*N*-alkyl-12-hydroxyoctadecylammonium salts, how mixed liquid systems affect the gelation processes, and perform experiments to glean additional details about the dynamics of the self-assembly of the NCl-*n* at the early stages of self-assembly. The ammonium part of the NCl-*n* will also be modified to place the hydroxyl at different positions along the octadecyl chain.

■ ASSOCIATED CONTENT

S Supporting Information. Materials sources, synthetic procedures, instrumentation, and characterization details, various POM images, comparison of XRD diffractograms of NCl-2 hydrogel with its neat gelator, pH stability of gels, comparison of T_{max} and ΔH from DSC thermograms, Schröder–van Laar plots, and SANS plots. This material is available free of charge via the Internet at <http://pubs.acs.org>.

■ AUTHOR INFORMATION

Corresponding Author

*E-mail: weissr@georgetown.edu.

■ ACKNOWLEDGMENT

We are grateful to the National Science Foundation for its support of this research, Dr. Jibao He and Professor Vijay John of Tulane University for recording the cryo-SEM images, Professor Daniel Blair of the Georgetown Physics Department for the use of his rheometer, and Dr. Boualem Hammouda of NIST for help with the SANS experiments. This work utilized facilities supported in part by the National Science Foundation under Agreement No. DMR-0454672. We acknowledge the support of the National Institute of Standards and Technology, U.S. Department of Commerce, in providing the neutron research facilities used in this work.

■ REFERENCES

- (1) (a) Shinkai, S.; Murata, K. *J. Mater. Chem.* **1998**, *8*, 485–495. (b) van Esch, J. H.; Feringa, B. L. *Angew. Chem., Int. Ed.* **2000**, *39*, 2263–2266. (c) Sangeetha, N. M.; Maitra, U. *Chem. Soc. Rev.* **2005**, *34*, 821–836. (d) *Molecular Gels. Materials with Self-Assembled Fibrillar Networks*; Weiss, R. G.; Terech, P., Eds.; Springer: The Netherlands, 2006. (e) George, M.; Weiss, R. G. *Acc. Chem. Res.* **2006**, *39*, 489–497.
- (2) (a) Liu, X. Y.; Sawant, P. D. *Adv. Mater.* **2002**, *14*, 421–426. (b) Aggeli, A.; Nyrkova, I. A.; Bell, M.; Harding, R.; Carrick, L.; McLeish, T. C. B.; Semenov, A. N.; Boden, N. *Proc. Natl. Acad. Sci.* **2001**, *98*, 11857–11862.
- (3) van Esch, J. H.; Schoonbeek, F.; Loos, M. D.; Veen, E. M.; Kellogg, R. M.; Feringa, B. L. In *Supramolecular Science: Where It Is and Where It Is Going*; Ungar, R., Dalcanale, E., Eds.; Kluwer Academic Publishers: The Netherlands, 1999, pp 233–259.
- (4) Shankar, R.; Ghosh, T. K.; Spontak, R. J. *Soft Matter* **2007**, *3*, 1116–1129.
- (5) Edwards, W.; Lagadec, C. A.; Smith, D. K. *Soft Matter* **2011**, *7*, 110–117.
- (6) George, M.; Weiss, R. G. In *Molecular Gels. Materials with Self-Assembled Fibrillar Networks*; Weiss, R. G., Terech, P., Eds.; Springer: The Netherlands, 2006, Chapter 14.
- (7) (a) Chen, J.; Kampf, J. W.; McNeil, A. J. *Langmuir* **2010**, *26*, 13076–13080. (b) Sahoo, P.; Adarsh, N. N.; Chacko, G. E.; Raghavan, S. R.; Puranik, V. G.; Dastidar, P. *Langmuir* **2009**, *25*, 8742–8750. (c) Piepenbrock, M.-O. M.; Lloyd, G. O.; Clarke, N.; Steed, J. W. *Chem. Commun.* **2008**, 2644–2646. (d) Terech, P.; Sangeetha, N. M.; Maitra, U. *J. Phys. Chem. B* **2006**, *110*, 15224–15233. (e) Makarević, J.; Jokić, M.; Raza, Z.; Stefanić, Z.; Kojić-Prodić, B.; Žinić, M. *Chem.—Eur. J.* **2003**, *9*, 5567–5580. (f) Abdallah, D. J.; Sirchio, S. A.; Weiss, R. G. *Langmuir* **2000**, *16*, 7558–7561.
- (8) Ostuni, E.; Kamaras, P.; Weiss, R. G. *Angew. Chem., Int. Ed.* **1996**, *35*, 1324–1326.
- (9) <http://www.ncnr.nist.gov/> (accessed May 2011).
- (10) Kline, S. R. *J. Appl. Crystallogr.* **2006**, *39*, 895–900.
- (11) Terech, P. In *Molecular Gels. Materials with Self-Assembled Fibrillar Networks*; Weiss, R. G.; Terech, P., Eds.; Springer: Dordrecht, The Netherlands, 2006, pp 275–324.
- (12) (a) Terech, P.; Pasquier, D.; Bordas, V.; Rossat, C. *Langmuir* **2000**, *16*, 4485–4494. (b) Tachibana, T.; Mori, T.; Hori, K. *Bull. Chem. Soc. Jpn.* **1980**, *53*, 1714–1719. (c) Tachibana, T.; Kambara, H. *J. Am. Chem. Soc.* **1965**, *87*, 3015–3016. (d) Huang, X.; Weiss, R. G. *Tetrahedron* **2007**, *63*, 7375–7385.
- (13) Mallia, V. A.; George, M.; Blair, D. L.; Weiss, R. G. *Langmuir* **2009**, *25*, 8615–8625.
- (14) (a) Marton, L.; McBain, J. W.; Vold, R. D. *J. Am. Chem. Soc.* **1941**, *63*, 1990–1993. (b) Zana, R. *Langmuir* **2004**, *20*, 5666–5668. (c) Novales, B.; Navilles, L.; Axelos, M.; Nallet, I.; Douliez, J.-P. *Langmuir* **2008**, *24*, 62–68.
- (15) (a) Sakurai, T.; Masuda, Y.; Sato, H.; Yamagishi, A.; Kawaji, H.; Atake, T.; Hori, K. *Bull. Chem. Soc. Jpn.* **2010**, *83*, 145–149. (b) Terech, P.; Rodriguez, V.; Barnes, J. D.; McKenna, G. B. *Langmuir* **1994**, *10*, 3406–3418. (c) Tamura, T.; Ichikawa, M. *J. Am. Oil Chem. Soc.* **1997**, *74*, 491–495. (d) Terech, P. *Colloid Polym. Sci.* **1991**, *269*, 490–500.
- (16) (a) Tachibana, T.; Kambara, H. *J. Am. Chem. Soc.* **1965**, *87*, 3015–3016. (b) Tachibana, T.; Kitazawa, S.; Takeno, H. *Bull. Chem. Soc. Jpn.* **1970**, *43*, 2418–2421.
- (17) (a) Douglas, J. F. *Langmuir* **2010**, *25*, 8386–8391. (b) Rogers, M. A.; Alejandro, G. *Langmuir* **2009**, *25*, 8556–8566. (c) Wang, R.-Y.; Liu, X.-Y. *Int. J. Nanosci.* **2006**, *5*, 645–649. (d) Wang, R. Y.; Liu, X.-Y.; Xiong, J. Y.; Li, J. L. *J. Phys. Chem. B* **2006**, *110*, 7275–7280. (e) Huang, X.; Terech, P.; Raghavan, S. R.; Weiss, R. G. *J. Am. Chem. Soc.* **2005**, *127*, 4336–4344. (f) Huang, X.; Terech, P.; Raghavan, S. R.; Weiss, R. G. *J. Am. Chem. Soc.* **2006**, *128*, 15341–15352. (g) Terech, P. *J. Colloid Interface Sci.* **1985**, *107*, 244–255.
- (18) (a) Estroff, L. A.; Hamilton, A. D. *Chem. Rev.* **2004**, *104*, 1201–1217. (b) Kiyonaka, S.; Shinkai, S.; Hamachi, I. *Chem.—Eur. J.* **2003**, *9*, 976–983. (c) Oda, R.; Huc, I.; Candau, S. J. *Angew. Chem., Int. Ed.* **1998**, *37*, 2689–2691. (d) Makarević, J.; Jokić, M.; Perić, B.; Tomisić, V.; Kojić-Prodić, B.; Žinić, M. *Chem.—Eur. J.* **2001**, *7*, 3328–3341. (e) Yan, N.; He, G.; Zhang, H.; Ding, L.; Fang, Y. *Langmuir* **2010**, *26*, 5909–5917. (f) Vemula, P. K.; Li, J.; John, G. *J. Am. Chem. Soc.* **2006**, *128*, 8932–8938.
- (19) This method has been employed by others previously: (a) Das, U. K.; Trivedi, D. R.; Adarsh, N.; Dastidar, P. *J. Org. Chem.* **2009**, *74*, 7111–7121. (b) Suzuki, M.; Nakajima, Y.; Yumoto, M.; Kimura, M.; Hirai, H.; Hanabusa, K. *Org. Biomol. Chem.* **2004**, *2*, 1155–1159. (c) Sahoo, P.; Kumar, D. K.; Raghavan, S. R.; Dastidar, P. *Chem.—Asian J.* **2011**, *6*, 1038–1047.
- (20) Lide, D. R. *Handbook of Organic Solvents*; CRC Press: London, 1995, pp 561–565.
- (21) Larson, R. G. *The Structure and Rheology of Complex Fluids*; Oxford University Press: Oxford, 1999, p 13.
- (22) (a) Hirst, A. R.; Coates, I. A.; Boucheteau, T. R.; Miravet, J. F.; Escuder, B.; Castelletto, V.; Hamley, I. W.; Smith, D. K. *J. Am. Chem. Soc.* **2008**, *130*, 9113–9121. (b) Mukkamala, R.; Weiss, R. G. *Langmuir* **1996**, *12*, 1474–1482. (c) Lu, L.; Cocker, T. M.; Bachman, R. E.; Weiss, R. G. *Langmuir* **2000**, *16*, 20–34.
- (23) Fages, F.; Vögtle, F.; Žinić, M. *Top. Curr. Chem.* **2005**, *256*, 77–131.
- (24) Wang, T.; Li, Y.; Liu, M. *Soft Matter* **2009**, *5*, 1066–1073.
- (25) Adams, D. J.; Morris, K.; Chen, L.; Serpell, L.; Bacsa, J.; Day, G. M. *Soft Matter* **2010**, *6*, 4144–4156.
- (26) (a) Lin, Y.; Kachar, B.; Weiss, R. G. *J. Am. Chem. Soc.* **1989**, *111*, 5542–5551. (b) Furman, I.; Weiss, R. G. *Langmuir* **1993**, *9*, 2084–2088.
- (27) Davey, R. J.; Garside, J. *From Molecules to Crystallizers*; Oxford University Press: New York, 2000, Chapter 2 and references cited therein.
- (28) Li, J.-L.; Liu, X.-Y. *J. Phys. Chem. B* **2009**, *113*, 15467–15472.
- (29) George, M.; Tan, G.; John, V. T.; Weiss, R. G. *Chem.—Eur. J.* **2005**, *11*, 3243–3255.
- (30) Liu, X.-Y.; Sawant, P. D. *Appl. Phys. Lett.* **2001**, *79*, 3518–3520.
- (31) Other factors, such as the fiber dimensions, fiber bundling, and the frequency and type of junction zones, must contribute, as well. Unfortunately, the limited SANS beam time did not allow them to be measured for the whole set of NCl_n .
- (32) Individual melting temperatures for the different gel phases (Supporting Information Table S2) could not be determined in some cases because of peak overlaps. These gel-to-gel transitions are an interesting phenomenon that will be explored in depth in the future.
- (33) A more pronounced manifestation of this phenomenon has been observed in the CCl_4 gels of (R) -18-(propylamino)-7-octadecanol, the amino alcohol from which NCl_3 was prepared. Mallia, V. A.; Butler, P. D.; Sarkar, B.; Holman, K. T.; Weiss, R. G. *J. Am. Chem. Soc.* **2011**, *133*, 15045–15054.
- (34) The enthalpies of the gel-to-sol transition of both the hydrogel and toluene gel of NCl_3 were also calculated using the Schröder–van Laar equation (see Supporting Information Figure S5).^{34a} They are significantly larger than the heat found directly for neat NCl_3 . The (incorrect) assumption of ideality of the sol phase is a probable

contributor to why this treatment fails to provide a reasonable result here. (a) Atkins, P. W. *Physical Chemistry*, 5th ed.; Freeman: New York, 1994, p 227. (b) Moore, W. J. *Physical Chemistry*, 4th ed.; Prentice Hall: Englewood Cliffs, NJ, 1972, p 249.

(35) Because the number of reflection peaks is relatively small and the signal-to-noise ratio of some diffractograms is low, the correspondence between the morphs must be taken with caution.

(36) Using JADE software from Materials Data Inc., Release 5.0.35 (SPS), Livermore, CA. Details regarding indexing the peaks of neat NCl-3 and its packing arrangements will be reported elsewhere.

(37) Using Chem 3 D Ultra 8 software (Cambridge Soft Corporation, Cambridge, MA, USA) and adding the van der Waals radii of the terminal atoms according to (a) Bondi, A. *J. Phys. Chem.* **1964**, *68*, 441–451. (b) Mantina, M.; Chamberlin, A. C.; Valero, R.; Cramer, C. J.; Truhlar, D. G. *J. Phys. Chem. A* **2009**, *113*, 5806–5812.

(38) Jung, J. H.; Shinkai, S.; Shimizu, T. *Chem.—Eur. J.* **2002**, *8*, 2684–2690.

(39) Israelachvili, J. N. *Intermolecular and Surface Forces*, 3rd ed; Academic Press: London, 1992.

(40) (a) Sawa, Y.; Ye, F. F.; Urayama, K.; Takigawa, T.; Gimenez-Pinto, V.; Selinger, R. L. B.; Selinger, J. V. *Proc. Natl. Acad. Sci.* **2011**, *108*, 6364–6368. (b) Brizard, A.; Oda, R.; Huc, I. In *Low Molecular Mass Gelators: Design, Self-Assembly, Function*; Topics in Current Chemistry; Fages, F., Ed; Springer-Verlag: Berlin, 2005; Vol. 256; pp 167–218. (c) van Gestel, J.; van der Schoot, P.; Michels, M. A. J. In *Molecular Gels. Materials with Self-Assembled Fibrillar Networks*; Weiss, R. G., Terech, P., Eds.; Springer: The Netherlands, 2006, Chapter 2. (d) Agelli, A.; Boden, N.; Carrick, L. M.; Mcleish, T. C. B.; Nyrkova, I. A.; Semenov, A. N. In *Molecular Gels. Materials with Self-Assembled Fibrillar Networks*; Weiss, R. G., Terech, P., Eds.; Springer: The Netherlands, 2006, Chapter 3.

(41) Terech, P.; Dourdain, S.; Bhat, S.; Maitra, U. *J. Phys. Chem. B* **2009**, *113*, 8252–8267.

(42) Debye, P.; Bueche, A. M. *J. Appl. Phys.* **1949**, *20*, 518–526.

(43) Carri, G. A.; Muthukumar, M. *J. Chem. Phys.* **1999**, *111*, 1765–1777.

(44) Terech, P.; Jean, B.; Ne, F. *Adv. Mater.* **2006**, *18*, 1571–1574.

(45) (a) Avrami, M. *J. Chem. Phys.* **1939**, *7*, 1103–1112. (b) Avrami, M. *J. Chem. Phys.* **1940**, *8*, 212.

(46) Mandelkern, L. *Crystallization of Polymers*; Cambridge University Press: Cambridge, 2004; vol 2; pp 18–19.

(47) Lam, R. S. H.; Rogers, M. A. *Cryst. Eng. Commun.* **2011**, *13*, 866–875.

(48) The corresponding value of K using eq 6, $0.013\text{ }(\text{s}^2)^{-1}$, is of little physical value without a larger body of rate constants with which to compare it. Unfortunately, we were unable to obtain additional rate data during the beam time allotted.

(49) (a) Abdallah, D. J.; Bachman, R. E.; Perlstein, J.; Weiss, R. G. *J. Phys. Chem. B* **1999**, *103*, 9269–9278. (b) Ma, K.; Minkova, L.; Lee, K.-M.; Weiss, R. G. *J. Org. Chem.* **2009**, *74*, 2088–2098.